▮ **Ruthenium Complexes** |*Hot Paper*|

HN$_2$O$_2^-$ as a Ligand in Mononuclear Hydrogenhyponitrite-κ^2-*N,O* Ruthenium Complexes with Bisphosphane Co-Ligands
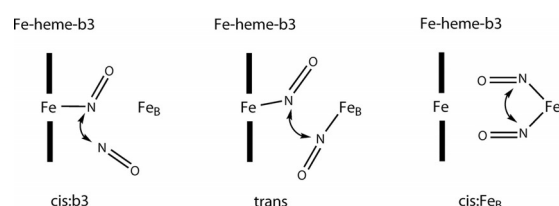
Daniel Beck and Peter Klüfers*[a]

Abstract: The hyponitrite anion is a tentative intermediate in the reduction of nitric oxide (NO) to nitrous oxide (N_2O) catalyzed by nitric-oxide reductase (NOR) in the process of bacterial denitrification. Owing to the considerable number of known coordination modes for the hyponitrito ligand, its actual bonding form in the enzymatic cycle is a point of current discussion. Here, we contribute to the hardly known ligand properties of a key intermediate, the monoprotonated hyponitrite anion. Three air- and water-stable ruthenium complexes with hydrogenhyponitrite as the ligand were synthesized by using commercially available bisphosphane co-ligands (1,2-bis(diphenylphosphino)ethane (dppe), 1,3-bis(diphenylphosphino)propane (dppp), 1,2-bis(diphenylphosphino)ethene (dppv)). The starting compounds [Ru(dppe)$_2$(tos)]BF$_4$ (**1**) and [Ru(dppp)$_2$(tos)]BF$_4$ (**2**) contained the bidentate coordinating tosylate anion (tos) as a particularly well-suited leaving group. To confirm the protonated and deprotonated species, X-ray diffraction, IR, UV/Vis spectroscopy (solution and solid state), solid-state NMR spectroscopy, and high-resolution mass spectroscopy were used. DFT calculations give insight into the bonding situation. We report on [Ru(dppe)$_2$(HN$_2$O$_2$)]BF$_4$ (**5**), [Ru(dppp)$_2$(HN$_2$O$_2$)]BF$_4$ (**6**), [Ru(dppv)$_2$(HN$_2$O$_2$)]BF$_4$ (**7**), [Ru(dppp)$_2$(HN$_2$O$_2$)]BF$_4$·Imi (**9**; Imi = imidazole) as the first mononuclear *trans*-hydrogenhyponitrite complexes. Isolated deprotonated analogs are [Ru(dppe)$_2$(N$_2$O$_2$)]·HImi(BF$_4$) (**8**) and [Ru(dppv)$_2$(N$_2$O$_2$)]·HImi(BF$_4$)·Imi (**10**).

Introduction

The nitrogen cycle is a fundamental process of nature in which nitrogen-containing species are fixed and released.[1] Denitrification, the reduction of nitrate by several enzymatic steps to elemental nitrogen ($NO_3^- \rightarrow NO_2^- \rightarrow NO \rightarrow N_2O \rightarrow N_2$) is undesired in agricultural fertilization, as the nutrient becomes unavailable for plants.[2,3] The enzyme NOR (nitric-oxide reductase) is present in bacteria and catalyzes the nitric-oxide-to-nitrous-oxide step.[4] The reduction step from nitric oxide to nitrous oxide provides pathogens such as *Neisseria gonorrhoeae* or *N. meningitidis* with a protection mechanism against the toxic NO molecule, which is released by mammalian NO synthase as part of the immune defense.[5–7]

The mechanism of NO reduction still remains unclear, but there are several indicators that a reactive hyponitrite intermediate is formed, which is transformed through two protonation steps to nitrous oxide ($N_2O_2^{2-} + 2H^+ \rightarrow N_2O + H_2O$). The most likely mechanism was derived from EPR spectroscopic experiments by using freeze-quench techniques by observing time-dependent EPR spectral changes. The tentative formation of ferrous Fe$_B$-NO and ferrous heme-b$_3$-NO in the same ratio support the formation of a hyponitrite intermediate through a *trans* mechanism (Scheme 1).[8] Nonetheless, calculations indicate that the intermediates that result from the *trans* mechanism are energetically unfavorable. A so-called *cis*:b$_3$ mechanism seems more reasonable, where one NO coordinates the heme-iron center (Fe-b$_3$) and gets attacked by a non-coordinating NO resulting in a *cis*-hyponitrite coordinated to the non-heme iron center.[9] The *cis*:Fe$_B$ mechanism derived from the rules of organometallic chemistry is of historic interest only.[10] However, presently, owing to the lack of structural information,

[a] D. Beck, Prof. Dr. P. Klüfers
Ludwig-Maximilians-Universitaet, Department of Chemistry
Butenandtstrasse 5–13, Haus D, München, 81377 (Germany)
E-mail: kluef@cup.uni-muenchen.de

Supporting information and the ORCID identification number(s) for the author(s) of this article can be found under:
https://doi.org/10.1002/chem.201803770.

Scheme 1. Proposed mechanisms of hyponitrite formation.[11]

a final conclusion is not possible, especially in terms of binding modes.

Scheme 2 highlights the fact that hyponitrite is discussed not only as an intermediate in the enzymatic process of NOR, but is also a ligand of current interest in other fields of coordination chemistry. Hence, nine coordination modes are known for the hyponitrito ligand in its *cis* or *trans* forms.[11,12] Mononuclear complexes are restricted to the *cis* type whereby both isomers are found in polynuclear complexes. Hyponitrite is able to bind up to four metal centers through each of its atoms.[12–16] Some characteristics of hyponitrite coordination
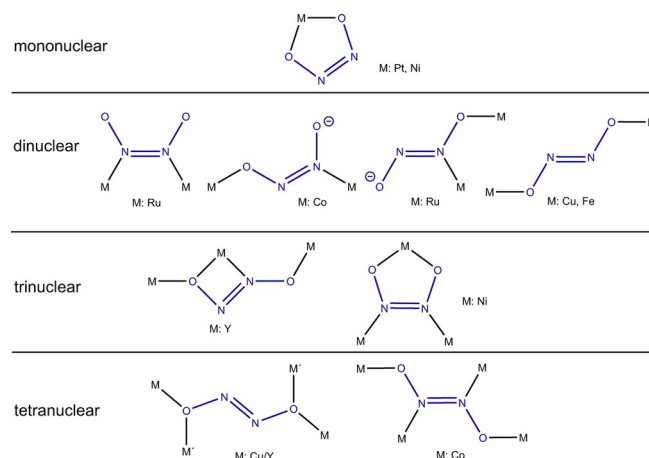
Scheme 2. Currently known hyponitrite binding modes.

are visible: the group 10 metals, nickel and platinum, provide a suitable environment for mononuclear *cis*-hyponitrito complexes.[13, 17] Cobalt, copper, iron, ruthenium, and yttrium form polynuclear *cis*- and *trans*-hyponitrito complexes.[12, 14–16, 18–20]

There is only one type of coordinated hydrogenhyponitrite known. Böttcher et al. synthesized a diruthenium(I) complex, bridged with sterically demanding phosphide ligands, which is capable of reducing nitric oxide to a bridging hyponitrite ligand according to $[Ru_2(CO)_4(\mu\text{-dppm})(\mu\text{-H})(\mu\text{-P}t\text{Bu}_2)] + 2\,NO \rightarrow [Ru_2(CO)_4(\mu\text{-dppm})(\mu\text{-H})(ONNO\text{-}1\kappa N\text{:}2\kappa O)(\mu\text{-P}t\text{Bu}_2)]$. Subsequent protonation led to a hydrogenhyponitrito complex, which released nitrous oxide upon heating.[20–22]

To get deeper insight into the coordination chemistry of the rare hydrogenhyponitrito ligand, we attempted the synthesis of mononuclear complexes of this tentative intermediate. Hence, we report here on the preparation and characterization of mononuclear phosphane-supported ruthenium complexes of the hydrogenhyponitrito ligand, that is, of a hyponitrite entity halfway towards N_2O formation.

Figure 1. ORTEP-3 plot (ellipsoids drawn at the 50% probability level) of the $[Ru(dppe)_2(tos)]^+$ ion in **1**.[25] Distances (Å) and angles (°): Ru1–O1 2.267(2), Ru1–O2 2.291(2), Ru1–P1 2.3815(8), Ru1–P2 2.3031(7), Ru1–P3 2.4481(8), Ru1–P4 2.3034(8), S1–O1 1.486(2), S1–O2 1.489(2); S1–O3 1.441(2); O1-Ru1-O2 62.37(7). Further data are summarized in the Supporting Information.

Results and Discussion

Ruthenium precursors with a weakly bonded leaving ligand

As the starting materials, we used the ruthenium complexes $[Ru(dppe)_2(tos)]BF_4\cdot CHCl_3$ (**1**) and $[Ru(dppp)_2(tos)]BF_4\cdot Et_2O$ (**2**) both of which exhibit a $\kappa^2 O,O'$ tosylato chelate. Compounds **1** and **2** were synthesized from hexaaquaruthenium(II) tosylate (tos) and the respective bisphosphanes 1,2-bis(diphenylphosphino)ethane (dppe)[23] and 1,3-bis(diphenylphosphino)propane (dppp; Scheme 3). The products were obtained in crystalline form by using the tetrafluoridoborate counterion and their structures were confirmed by X-ray diffraction. The ruthenium(II) center was coordinated distorted-octahedrally by two bisphosphanes and a tosylato ligand, the latter being part of a four-ring chelate (Figure 1 and Figure 2). In comparison to known literature on complexes with *cis* dppe chelates, this synthesis had fewer steps and the product was obtained in quantitative yield.[24]
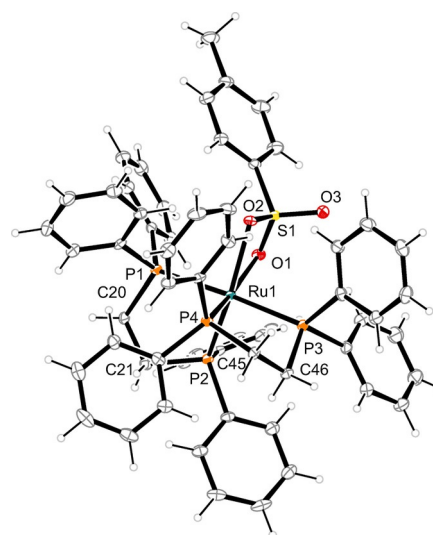
In addition, $[Ru(dppv)_2(H_2O)_2](BF_4)_2$ (**3**) was used as a starting material and synthesized according to the methods used for **1** and **2**. The octahedral complex consists of two apical 1,2-bis(diphenylphosphino)ethene (dppv) bisphosphane ligands and two axial aqua ligands coordinated to the ruthenium(II) center (Figure 3).

Room-temperature powder diffractograms and high-resolution mass spectra confirmed the formation of pure **1** and **2**, whereby **3** was a mixture of a mainly coarsely crystalline phase and several different microcrystalline phases. Infrared spectra showed sharp signals at 1256 cm^{-1} (**1**) and 1249 cm^{-1} (**2**) for the tosylato ligand (free tosylate: 1200 cm^{-1}).[23] Further analytics (NMR, UV/Vis, IR spectra) confirmed the formation of the complexes **1**–**3** (see the Supporting Information). For the following reactions, the starting materials were used without further purification.
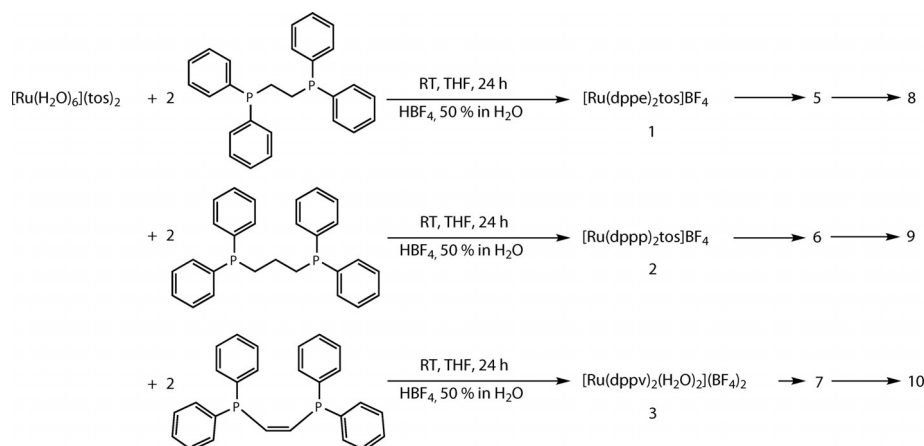
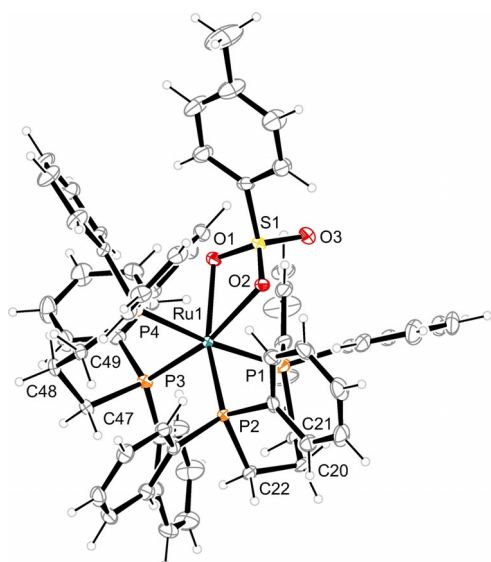**Scheme 3.** Formation of the starting materials **1**–**3** and their use in subsequent transformations.

Figure 2. ORTEP-3 plot (ellipsoids drawn at the 50% probability level) of the [Ru(dppp)₂(tos)]⁺ ion in **2**.[25] Distances (Å) and angles (°): Ru1—O1 2.311(2), Ru1—O2 2.255(2), Ru1—P1 2.4770(8), Ru1—P2 2.3124(7), Ru1—P3 2.3210(8), Ru1—P4 2.4331(7), S1—O1 1.480(2), S1—O2 1.488(2), S1—O3 1.442(2); O1-Ru1-O2 62.10(7). Further data are summarized in the Supporting Information.
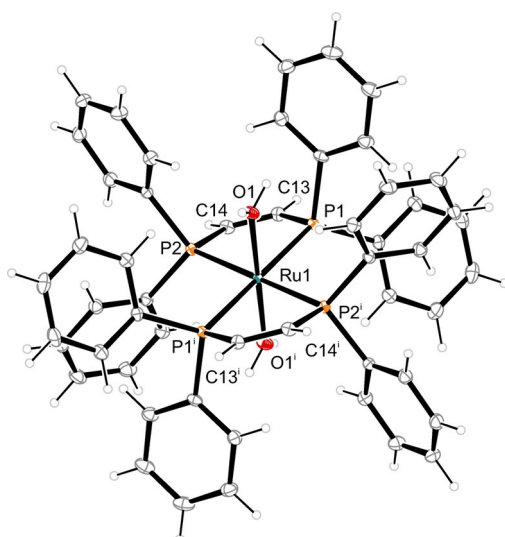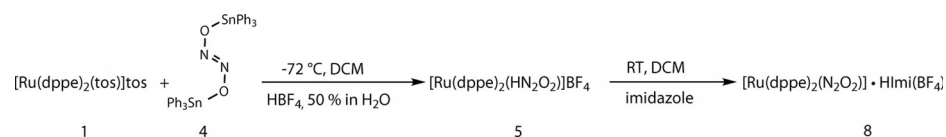

Figure 3. ORTEP-3 plot (ellipsoids drawn at the 50% probability level) of the [Ru(dppv)₂(H₂O)₂]²⁺ ion in **3**.[25] Distances (Å) and angles (°): Ru1—O1 2.1252(12), Ru1—P1 2.3641(4), Ru1—P2 2.3849(4); P1-Ru1-P2 82.34(2).

Hydrogenhyponitrito complexes

Cooled solutions of the starting materials **1–3** were treated with triphenylstannyl hyponitrite **4** to obtain the hydrogenhy-

ponitrito complexes **5–7** [Ru(dppe)₂(HN₂O₂)]BF₄·Et₂O (**5**, Scheme 4), [Ru(dppp)₂(HN₂O₂)]BF₄·Et₂O (**6**), [Ru(dppv)₂(HN₂O₂)]-BF₄·0.81 TBME (**7**; TBME = *tert*-butylmethyl ether). Triphenyl-stannyl hyponitrite was used as a synthon as the use of sodium or silver *trans*-hyponitrite was unsuccessful. Compounds **5–7** represent the first mononuclear *trans*-hydrogenhy-ponitrite complexes ever synthesized. The protonation must be done prior to the isolation steps, otherwise the products did not crystallize. In general, the tosylato ligand was substitut-ed by the hydrogenhyponitrito ligand under formation of a four-ring chelate with the ruthenium(II) center. The bisphos-phane ligands arranged themselves in a *cis* position to com-plete the distorted octahedra (Figure 4, Figure 5, Figure 6). The hydrogenhyponitrito ligand resembles *trans*-H₂N₂O₂ and the *trans*-N₂O₂²⁻ anion in the sodium salt in terms of bond lengths, whereas the angles about the nitrogen atoms are enlarged for the hydroxy-bonding N, and diminished for the chelate-N (Table 1).[26]

High-resolution mass spectra confirm the formation of the hydrogenhyponitrito complexes **5–7**. We detected the *trans*-hyponitrito ligand by infrared spectroscopy as the N=N vibra-tion is spectroscopically allowed owing to the asymmetrical bonding pattern. Frequencies are shown in Table 2 and com-pared with the computationally determined values. Solution NMR spectroscopy showed more signals than expected for the bisphosphanes, probably owing to solution equilibria including
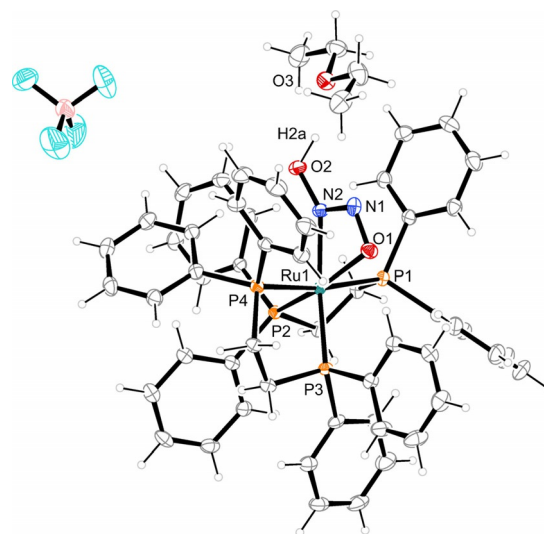

Figure 4. ORTEP-3 plot (ellipsoids drawn a the 50% probability level) of [Ru(dppe)₂(HN₂O₂)]BF₄·Et₂O (**5**).[25] Distances (Å) and angles (°): Ru1—N2 2.151(2), Ru1—O1 2.173(2), Ru1—P1 2.3875(6), Ru1—P2 2.3357(6), Ru1—P3 2.3229(6), Ru1—P4 2.3725(6); N2-Ru1-O1 56.92(7), N1-O1-Ru1 96.77(13), N1-N2-Ru1 99.53(15), O2-N2-Ru1 144.55(15). Further data are summarized in the Supporting Information and in Table 1.
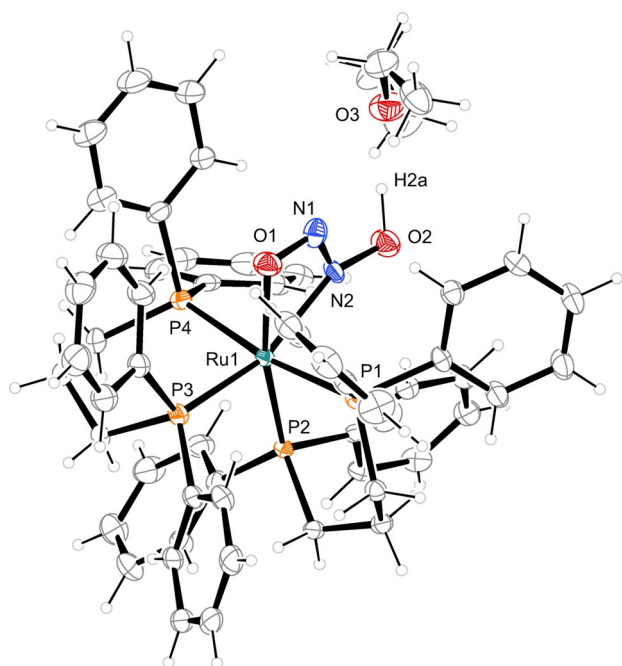

Scheme 4. Formation of **5** and **8**.

Figure 5. ORTEP-3 (ellipsoids drawn at the 50% probability level) of [Ru(dppp)₂(HN₂O₂)]BF₄·Et₂O·**DCM** (**6**).[25] The tetrafluoridoborate counterion and and the DCM crystal solvent have been omitted. Distances (Å) and angles (°): Ru1–N2 2.201(3), Ru1–O1 2.137(2), Ru1–P1 2.4144(9), Ru1–P2 2.3404(8), Ru1–P3 2.3183(9), Ru1–P4 2.4112(9); N2-Ru1-O1 56.99(11), N1-O1-Ru1 97.4(2), N1-N2-Ru1 96.6(2), O2-N2-Ru1 150.1(2). Further data are summarized in the Supporting Information and in Table 1.
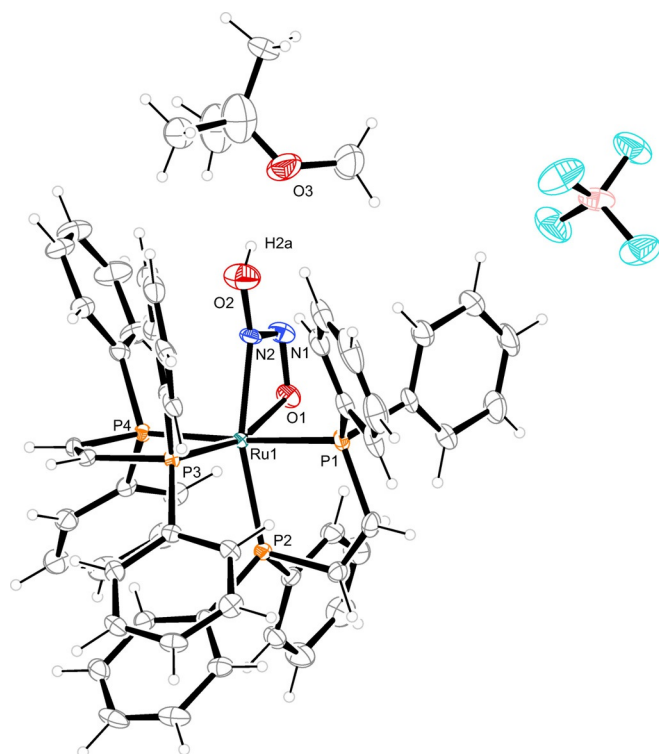

Figure 6. ORTEP-3 plot (ellipsoids drawn at the 50% probability level) of [Ru(dppv)₂(HN₂O₂)]BF₄·0.81 TBME (**7**).[25] The crystal solvent, except hydrogen-bonded TBME, has been omitted. Distances (Å) and angles (°): Ru1–N2 2.120(3), Ru1–O1 2.163(3), Ru1–P1 2.3465(11), Ru1–P2 2.3025(11), Ru1–P3 2.2885(10), Ru1–P4 2.3510(11); N2-Ru1-O1 58.68(13), N1-O1-Ru1 95.8(2), N1-N2-Ru1 99.8(3), O2-N2-Ru1 146.5(3). Further data are summarized in the Supporting Information and in Table 1.

Table 1. Overview of bond lengths [Å] and angles [°] of free hyponitrite fragments from Ref. [26] and the products of this work. Further details are shown in the Supporting Information.

Compound	Fragment/ ligand	N≡N [Å]	N—O [Å]	N-N-O [°]
[HEt₂NCH₂CH₂NEt₂H] [HN₂O₂]·H₂N₂O₂ [26]	H₂N₂O₂ HN₂O₂⁻	1.226(4) 1.232(3)	1.363(3) 1.371(3) (-O-) 1.402(3) (-OH)	109.9(3) 110.1(2) (-O-) 108.2(2) (-OH)
Na₂N₂O₂·5H₂O [26]	N₂O₂²⁻	1.256(2)	1.3622(11)	112.14(9)
Protonated compounds				
5	HN₂O₂⁻	1.258(3)	1.309(3) (-O-Ru) 1.384(3) (-OH)	106.77(19) (-O-Ru) 115.72(19) (-OH)
6	HN₂O₂⁻	1.236(4)	1.307(4) (-O-Ru) 1.380(4) (-OH)	109.0(3) (-O-Ru) 113.3(3) (-OH)
7	HN₂O₂⁻	1.287(5)	1.346(5) (-O-Ru) 1.343(5) (-OH)	105.7(3) (-O-Ru) 113.6(3) (-OH)
9	HN₂O₂⁻	1.263(3)	1.348(3) (-O-Ru) 1.370(3) (-OH)	105.74(18) (-O-Ru) 113.72(18) (-OH)
Deprotonated compounds				
8	N₂O₂²⁻	1.260(3)	1.369(3) (-O-Ru) 1.345(3) (-O-)	104.7(2) (-O-Ru) 116.0(2) (-O-)
10	N₂O₂²⁻	1.268(3)	1.383(2) (-O-Ru) 1.323(2) (-O-)	105.71(17) (-O-Ru) 117.06(18) (-O-)

Table 2. Overview of infrared vibrations [cm⁻¹] of **5**–**10**. The (unscaled) theoretical frequencies were calculated with Orca4 at the BP86/def2-TZVP level of theory including Grimme's van der Waals correction (D3).[27]

	N—O stretching vibration [cm⁻¹]			N≡N stretching vibration [cm⁻¹]	
Protonated compounds	Found	Calcd	Assignment	Found	Calcd
[Ru(dppe)₂(HN₂O₂)]BF₄ (**5**)	715	709	O↔N-N	1311	1310
	1032	1035	O↔N-N	1450	1455
	1100	1109	N↔O-Ru		
[Ru(dppp)₂(HN₂O₂)]BF₄ (**6**)	730	715	O↔N-N	1313	1314
	1023	1022	O↔N-N	1453	1453
	1115	1122	N↔O-Ru		
[Ru(dppv)₂(HN₂O₂)]BF₄ (**7**)	718	707	O↔N-N	1313	1307
	1035	1035	O↔N-N		1453
	1112	1112	N↔O-Ru		
[Ru(dppp)₂(HN₂O₂)]BF₄ (**9**)	734	714	O↔N-N	1313	1313
	1020	1027	O↔N-N	1453	1451
	1131	1131	N↔O-Ru		
Deprotonated compounds					
[Ru(dppe)₂(N₂O₂)]·(HImi)BF₄ (**8**)	717	730	O↔N-N	1252	1252
	943	943	N↔O-Ru	1390	1386
[Ru(dppv)₂(N₂O₂)]·(HImi)BF₄·(Imi) (**10**)	716	716	O↔N-N	1253	1253
	935	939	N↔O-Ru	1385	1385

ligand exchange. Therefore, ³¹P{¹H} solid-state NMR spectroscopy was performed, and the expected number of four signals for the phosphorous atoms was obtained. Further analytics are collected in the Supporting Information.

The dominant motif of all the complexes is a rather short hydrogen bond between a hydrogenhyponitrite donor and an

ether acceptor (diethyl ether or *tert*-butylmethyl ether, TBME). In comparison, Böttcher's dinuclear complexes contain a hydrogen bond from the ligand to a tetrafluoridoborate counterion or a carbonyl co-ligand.[21,22] If **5** is crystallized from toluene/CH_2Cl_2 instead of diethyl ether/CH_2Cl_2, a hydrogen bond is formed to the tetrafluoridoborate anion as in Böttcher's case (Table 3).

As far as possible, the positional parameters of the hydrogenhyponitrite hydrogen atoms were refined freely, together with an individual isotropic displacement parameter.

Table 3. Overview of the hydrogen bonds formed in the products **5–10** by the hydrogen hyponitrite moiety and an ether, a tetrafluoridoborate anion, or imidazole.

Compound	D—H···A	D—H [Å]	H···A [Å]	D—A [Å]	Angle D-H···A [°]
Protonated compounds					
5	O2—H2A···O3	1.05(3)	1.63(3)	2.639(3)	159(3)
6	O2—H2A···O3	1.12(5)	1.62(5)	2.663(4)	151(4)
7	O2—H2A···O3	0.93(2)	1.80(4)	2.629(6)	148(6)
9	O2—H1···N3	0.99(4)	1.66(4)	2.6929(3)	165(4)
	N4—H2···F2	0.88(5)	1.90(5)	2.768(3)	172(4)
[Ru(dppe)$_2$(HN$_2$O$_2$)]BF$_4$ without solvent (**5b**)	O2—H2A···F1	0.74(5)	2.01(5)	2.674(3)	150(6)
Deprotonated compounds					
8	N4—H7···O1	0.88[a]	1.66	2.520(3)	166.2
10	N3—H62···O2	0.92(2)[b]	1.65(2)	2.567(3)	174(4)
	N4—H64···N6	0.88[a]	1.95	2.801(3)	161.1
	N5—H60···O1[c]	0.91(2)[b]	1.92(2)	2.800(3)	164(4)

[a] Constraint refinement. [b] Restraint refinement. [c] Symmetry key: $-x+1, -y+1, -z+2$.

Deprotonation experiments

To get deeper insight into the acid–base chemistry of the coordinated hydrogenhyponitrite anion, solutions of **5–7** and excess imidazole were prepared in CH_2Cl_2. Subsequent crystallization by solvent diffusion led to the products **8–10** (Figure 7, Figure 8, Figure 9).

As a result, the weak base imidazole (pK_b: 6.95, 25 °C, H_2O) was able to deprotonate **8** and **10**, but not **9**.[28] The dppp ligand had a higher electron density located at the phosphorous ligand as indicated by a larger high-field NMR shift in **6** compared with **5** and **7**. This, probably, led to an overall increase of the basicity of the hyponitrite moiety. Nonetheless, the hydrogen bond was maintained by the imidazole acceptor. In **9**, the ether acceptor was exchanged by the imidazole acceptor (O2—H1···N3). In **10**, a complex hydrogen-bond system was formed by imidazolium and imidazole (Figure 10). In contrast, **8** was a fragment of **9** forming only one hydrogen-bond (N4—H7···O1).
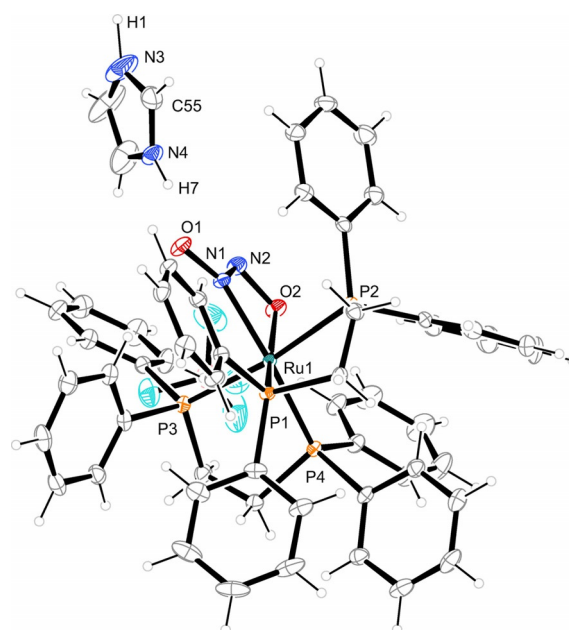

Figure 7. ORTEP-3 plot (ellipsoids drawn at the 50 % probability level) of [Ru(dppe)$_2$(N$_2$O$_2$)]·HImi(BF$_4$) (**8**).[25] Distances (Å) and angles (°): Ru1—N1 2.125(2), Ru1—O2 2.144(2), Ru1—P1 2.3402(7), Ru1—P2 2.3712(7), Ru1—P3 2.3708(7), Ru1—P4 2.3351(7); N1-Ru1-O2 58.40(8), O1-N1-Ru1 95.8(2), N2-N1-Ru1 100.7(2), O1-N1-Ru1 142.9(2), N1-N2-O2 104.7(2). Further data are summarized in the Supporting Information and in Table 1.
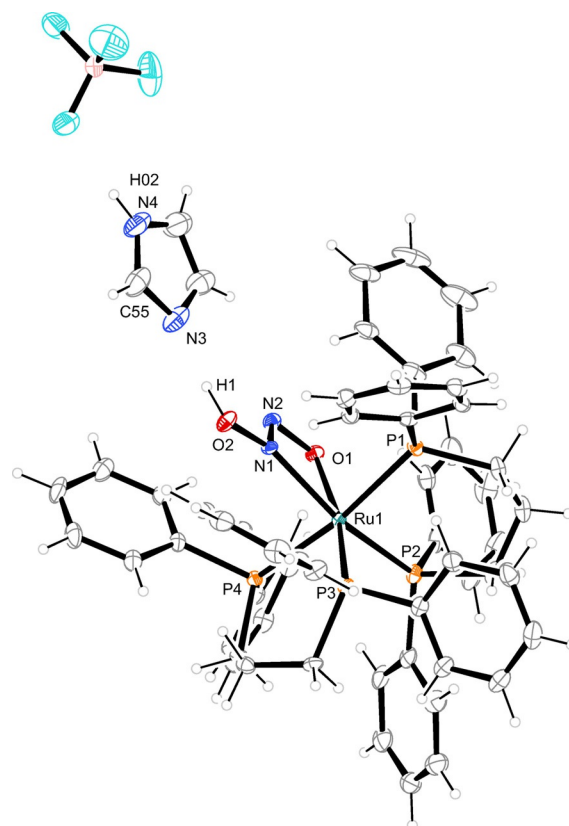

Figure 8. ORTEP-3 (ellipsoids drawn at the 50 % probability level) of [Ru(dppp)$_2$(HN$_2$O$_2$)]BF$_4$·Imi·0.856 CH$_2$Cl$_2$ (**9**).[25] Crystal solvent has been omitted. Distances (Å) and angles (°): Ru1—N1 2.194(2), Ru1—O1 2.135(2), Ru1—P1 2.4147(6), Ru1—P2 2.3100(6), Ru1—P3 2.3513(6), Ru1—P4 2.4062(6); N1-Ru1-O1 57.48(7), N2-O1-Ru1 98.40(12), N2-N1-Ru1 98.38(14), O2-N1-Ru1 147.86(15). Further data are summarized in the Supporting Information and in Table 1.
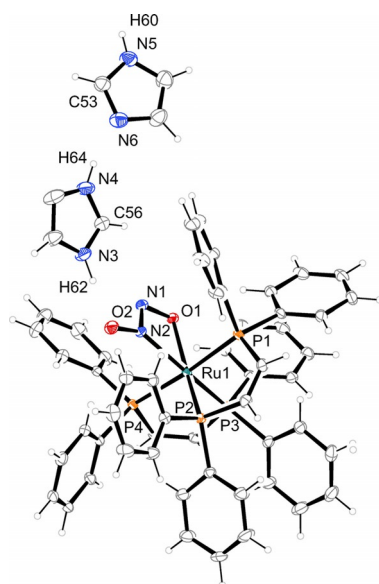
Figure 9. ORTEP-3 plot (ellipsoids drawn at the 50% probability level) of [Ru(dppv)$_2$(N$_2$O$_2$)]·HImi(BF$_4$)·Imi·0.804 CH$_2$Cl$_2$ (**10**).[25] The tetrafluoridoborate counterion and crystal solvent have been omitted. Distances (Å) and angles (°): Ru1−N2 2.124(28), Ru1−O1 2.149(2), Ru1−P1 2.3402(6), Ru1−P2 2.3036(6), Ru1−P3 2.2846(6), Ru1−P4 2.3469(6); N2-Ru1-O1 59.31(7), N1-O1-Ru1 95.01(11), N1-N2-Ru1 99.94(13), O2-N2-Ru1 142.54(15). Further data are summarized in the Supporting Information and in Table 1.
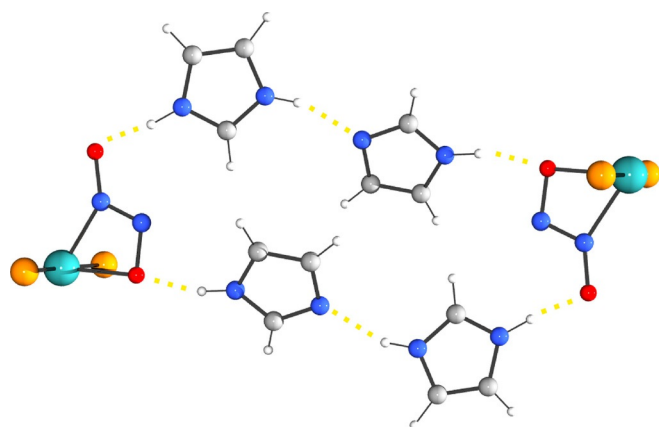

Figure 10. The hydrogen-bond network of **10**. Reduced illustration of the complex cation. Gray: carbon, blue: nitrogen, white: hydrogen, cyan: ruthenium, orange: phosphorus.

Difference Fourier analysis

As the determination of a hydrogen position in a routine X-ray analysis shows methodological limitations, additional information was desirable to settle the assignments. Thus, the deprotonation of **5** and **7** to yield **8** and **10**, as well as the non-deprotonation in **6**/**9**, was assured by further experimental data such as IR frequencies (Table 2) and color changes (Table 4).

However, even the X-ray method itself allowed us to derive a particularly reliable assignment in the case of **9** where a data set of very good quality was obtained. Figure 11 and Table 5 thus show the result of a ΔF analysis, prior to the H atom's assignment, in terms of the residual density's height and position

Table 4. Overview of the color changes before and after the addition of imidazole.

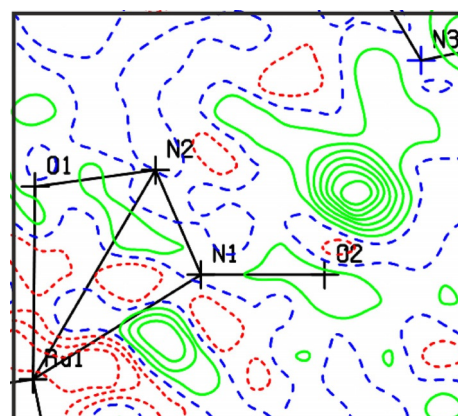| Transition	Color change
5→8	red-orange→yellow
6→9	brown-red→brown-red
7→10	yellow→pale yellow

Figure 11. Difference Fourier map of **9** around the hyponitrite/imidazole couple.

Table 5. Position and height of the residual density in the absence of the respective hydrogen atom together with the position after the refinement and the temperature factor of the hydrogen atom in **9**.

Difference Fourier peak	Distance from O2	Refined distance	U_{iso}
0.77 e Å^{-3}	0.947 Å	0.994(4) Å	0.055(12) Å^2

along the tentative hydrogen bond. In addition, Table 5 shows the result of the subsequent least-squares refinement with the positional parameters and an individual isotropic temperature parameter of the hydrogen atom as the refined parameters. The match of both algorithms is clear.

Bonding in the cation of 5, [Ru(dppe)$_2$(HN$_2$O$_2$)]$^+$

An ideally octahedral low-spin d^6 complex is expected to exhibit three doubly occupied t$_{2g}$ orbitals and two virtual e$_g$ orbitals, the latter showing metal–ligand σ-antibonds. The contributions to the former depend on the ligand characteristics: pure σ-donor ligands leave them metal-centered nonbonding; π-donor ligands result in metal–ligand π-antibonds with the contributing occupied molecular orbitals (MOs) mostly ligand-centered. Eventually, π-acceptor ligands lead to metal–ligand π-bonds with the empty ligand MOs usually intraligand π-antibonding.

Within this conceptual framework, the frontier-orbital region showed the signature of a σ- and π-donating HN$_2$O$_2$$^-$ ligand without considerable π-acceptor capability. Taking the P-Ru-P axis as z (Figure 12, top), the expected virtual, e$_g$-derived N/O-
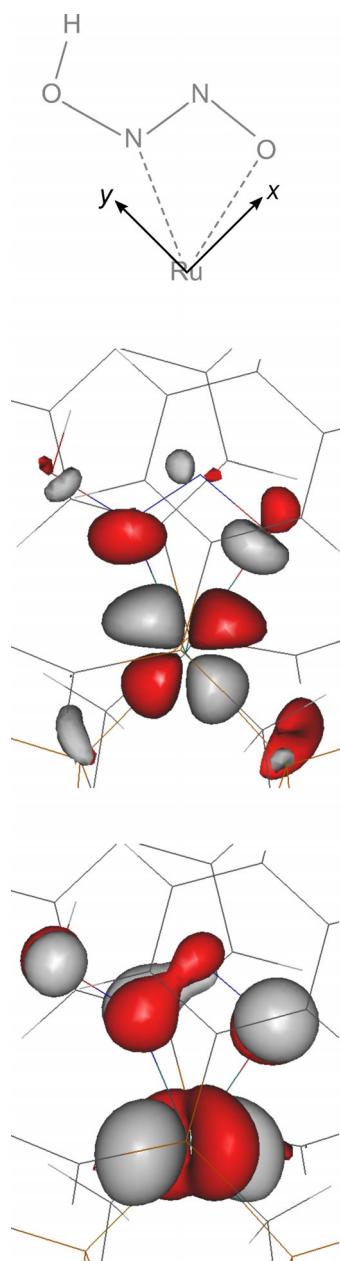
Figure 12. Gabedit plot of the frontier orbitals of the [Ru(dppe)$_2$(HN$_2$O$_2$)]$^+$ ion (isovalue: 0.05).[29] Top: choice of the Cartesian axes (z towards the observer); middle: the LUMO; bottom: the HOMO.

Ru σ-antibond was the LUMO and contained the Ru d(x^2-y^2) orbital as the metal part (Figure 12, middle). Two of the three occupied frontier MOs, specifically the HOMO−1 and the HOMO−2, showed mainly Ru d character in agreement with the σ character of the Ru−P interactions. The HOMO was made up from the HOMO−1 of the free hydrogenhyponitrito ligand in an antibond to the remaining t$_{2g}$-derived orbital. Specifically, with the axes chosen in Figure 12 (top), the HOMO was a linear combination of d(xz) and d(yz) (Figure 12, bottom). Thus, with its antibond between the metal orbital and an occupied ligand MO, the HOMO reflected the π-donor properties of the HN$_2$O$_2^−$ ligand. (The intraligand-π-MO contribution to the HOMO was N−N bonding but had nodes to both participating

oxygen p AOs.) As a result, the hydrogenhyponitrite anion shows the characteristics of a π-donating weak-field ligand.

The stability of the title compounds was not in line with the usual classification of the hydrogenhyponitrite ion as an intermediate towards nitrous-oxide formation.[12, 18, 19, 30] However, a closer look at space-filling models of **5–7** showed that the phenyl groups of the bisphosphane ligands enclosed the hydrogenhyponitrite/hyponitrite ligand and the ruthenium(II) center (Figure 13).
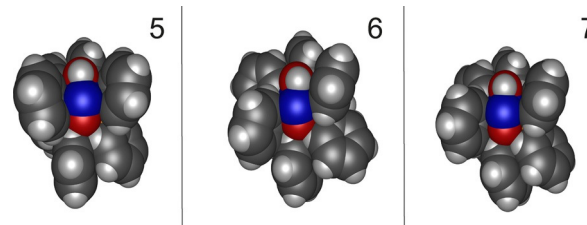

Figure 13. Space-filling model of the cations of **5–7** (Gabedit).[29]

Eventually, we tried to attain the hyponitrito ligand by the reductive coupling of nitric oxide, but all attempts were unsuccessful. Instead of hyponitrite formation, the starting complexes **1–2** showed tendencies to trigonal-bipyramidally coordinate a nitric oxide ligand. These nitrosyl complexes, however, have already been described.[31, 32]

Conclusion

We synthesized three mononuclear *trans*-hydrogenhyponitrito complexes with ruthenium. The *trans*-hydrogenhyponitrito-κ^{2}N,O ligands formed four-ring chelates with the ruthenium centers. Hydrogen bonds formed by a hydrogenhyponitrite donor to ether, fluoridoborate, or imidazole acceptors were a dominant motif in all of the crystal structures, whereby the hydrogenhyponitrito ligands of two of the three compounds were deprotonated by the weak base imidazole. DFT calculations confirmed the structures and revealed hydrogenhyponitrite to be a π-donor weak-field ligand.

Both the hydrogenhyponitrito, in general, and the *trans*-hyponitrito complexes are the first mononuclear species of their respective kinds reported. Future work will be directed towards N$_2$O release from the new compounds which, in terms of initial experiments, in fact, release nitrous oxide.

Experimental Section

Synthetic procedures

Hexaaquaruthenium(II) tosylate was prepared according to the literature.[33] All reactions were carried out under argon atmosphere. Silver hyponitrite as the source of bis(triphenylstannyl) hyponitrite was prepared according to the literature and stored for further use at 4 °C in the absence of light.[26, 34] The transformation of the starting material **1** to the hydrogenhyponitrito complex **5**, and, subsequently, to the hyponitrite complex **8**, is chosen as an example below. Detailed working instructions as well as analytical data and

additional structural parameters of all compounds are collected in the Supporting Information.

Synthesis of starting material 1 (tosylato complex)

A suspension of $[Ru(H_2O)_6](tos)_2$ (275 mg, 0.50 mmol, 1.00 equiv) and dppe (400 mg, 1.00 mmol, 2.00 equiv) in THF (10 mL) was stirred for 24 h. The solvent was removed and the crude product was suspended in dichloromethane (CH_2Cl_2). To this suspension, HBF_4 (126 µL, 2.00 equiv, 50% in water) was added. After filtration through a syringe filter, the solution was layered with diethyl ether. After crystallization and removal of the residual solvent, the crystals were washed three times with cyclohexane (10 mL each) and dried in vacuo. A yield of 520 mg (82% of theory) was obtained as orange crystals. (For the subsequent steps, the crude product can be used without problems.) Compounds **2** and **3** were synthesized in the same manner and are described in the Supporting Information.

Synthesis of the hydrogenhyponitrito complex 5

Crude **1** was dissolved in CH_2Cl_2 (15 mL) and cooled to $-72\,°C$. Bis(-triphenylstannyl) hyponitrite (**4**) was dissolved in CH_2Cl_2 (20 mL) and added dropwise to the solution of **1**. The light-yellow solution was stirred for 2 h and brought to room temperature afterwards. To the well-stirred solution, 600 µL HBF_4 (excess, 50% in water) was added and stirred until the solution became a suspension (ca. 15 min). The suspension was concentrated to 4 mL. The colorless solid was removed by filtration through a syringe filter, the solution was layered with diethyl ether and stored without any disturbance. Within 5 days, red blocks of **5** formed as well as colorless precipitate of, tentatively, tin-containing side products. The mother liquor was pipetted off and the colorless solid was removed by washing with diethyl ether (3×10 mL). The crystals were recrystallized with the same mixture of CH_2Cl_2 and diethyl ether, washed, and dried in vacuo. A yield of 439 mg (0.40 mmol, 80%) was obtained as red-orange crystals. Compounds **6** and **7** were synthesized in the same manner and are described in the Supporting Information.

Synthesis of the hyponitrito complex 8

Crystals of **5** (432 mg, 0.39 mmol) were dissolved in CH_2Cl_2 (5 mL) and imidazole (100 mg, excess) was added. The solution was filtered and layered with diethyl ether. When the color of the mother liquor remained constant (ca. 4 days), the mother liquor was pipetted off and the product was washed with diethyl ether (3×10 mL) and dried in vacuo. A yield of 361 mg (83%) was obtained as light-yellow crystals. Compounds **9** and **10** were synthesized in the same manner and are described in the Supporting Information.

Crystallography

Crystals were selected by using a Leica MZ6 polarization microscope. Suitable crystals were measured with a Bruker D8 Venture diffractometer using $Mo_{Kα}$ irradiation ($\lambda = 0.71073$ Å). Multi-scan absorption correction was applied. The structure solutions were carried out by direct methods by using SHELXT. The structures were refined by full-matrix least-squares calculations on F^2 by using SHELXL-2014.[35,36] Details are collected in the Supporting Information.

CCDC 1857075 (**1**), 1857076 (**5**), 1857077 (**8**), 1857078 (**5b**), 1857079 (**6**), 1857080 (**3**), 1857081 (**7**), 1857082 (**2**), 1857083 (**10**), and 1857120 (**9**) contain the supplementary crystallographic data for this paper. These data can be obtained free of charge from The Cambridge Crystallographic Data Centre.

Computational chemistry

All quantum-chemical calculations at the DFT level were performed with Orca4. Initial geometries were taken from crystal-structure analyses. Wave functions were calculated at the multipole-accelerated RI-DFT level by using def2-TZVP basis sets and the BP86 functional; dispersion correction was applied by using Grimme's DFT-D3 with BJ-damping as implemented in Orca4.[27] Frequency analyses were done numerically.

Conflict of interest

The authors declare no conflict of interest.

[1] N. Lehnert, J. C. Peters, *Inorg. Chem.* **2015**, *54*, 9229–9233.
[2] J. Wang, D. R. Chadwick, Y. Cheng, X. Yan, *Sci. Total Environ.* **2018**, *616–617*, 908–917.
[3] D. E. Canfield, A. N. Glazer, P. G. Falkowski, *Science* **2010**, *330*, 192–196.
[4] Y. Shiro, *Biochim. Biophys. Acta* **2012**, *1817*, 1907–1913.
[5] T. C. Householder, E. M. Fozo, J. A. Cardinale, V. L. Clark, *Infect. Immun.* **2000**, *68*, 5241–5246.
[6] M. F. Anjum, T. M. Stevanin, R. C. Read, J. W. B. Moir, *J. Bacteriol.* **2002**, *184*, 2987–2993.
[7] T. Hino, S. Nagano, H. Sugimoto, T. Tosha, Y. Shiro, *Biochim. Biophys. Acta* **2012**, *1817*, 680–687.
[8] H. Kumita, K. Matsuura, T. Hino, S. Takahashi, H. Hori, Y. Fukumori, I. Morishima, Y. Shiro, *J. Biol. Chem.* **2004**, *279*, 55247–55254.
[9] M. R. Blomberg, *Biochemistry* **2017**, *56*, 120–131.
[10] R. W. Ye, B. A. Averill, J. M. Tiedje, *Appl. Environ. Microbiol.* **1994**, *60*, 1053–1058.
[11] A. M. Wright, T. W. Hayton, *Inorg. Chem.* **2015**, *54*, 9330–9341.
[12] D. Lionetti, G. de Ruiter, T. Agapie, *J. Am. Chem. Soc.* **2016**, *138*, 5008–5011.
[13] S. Bhaduri, B. F. G. Johnson, A. Pickard, P. R. Raithby, G. M. Sheldrick, C. I. Zuccaro, *J. Chem. Soc. Chem. Commun.* **1977**, 354–355.
[14] H.-C. Böttcher, P. Mayer, *Inorg. Chim. Acta* **2010**, *363*, 799–801.
[15] W. J. Evans, M. Fang, J. E. Bates, F. Furche, J. W. Ziller, M. D. Kiesz, J. I. Zink, *Nat. Chem.* **2010**, *2*, 644–647.
[16] R. Bau, I. H. Sabherwal, A. B. Burg, *J. Am. Chem. Soc.* **1971**, *93*, 4926–4928.
[17] A. M. Wright, G. Wu, T. W. Hayton, *J. Am. Chem. Soc.* **2012**, *134*, 9930–9933.
[18] G. B. Wijeratne, S. Hematian, M. A. Siegler, K. D. Karlin, *J. Am. Chem. Soc.* **2017**, *139*, 13276–13279.
[19] N. Xu, E. G. Abucayon, D. R. Powell, G. B. Richter-Addo, *Nitric Oxide* **2016**, *52*, 16–20.
[20] T. Mayer, P. Mayer, H.-C. Böttcher, *J. Organomet. Chem.* **2012**, *700*, 41–47.

[21] H.-C. Böttcher, M. Graf, K. Mereiter, K. Kirchner, *Organometallics* **2004**, *23*, 1269–1273.

[22] H.-C. Böttcher, C. Wagner, K. Kirchner, *Inorg. Chem.* **2004**, *43*, 6294–6299.

[23] O. H. Bailey, A. Ludi, *Inorg. Chem.* **1985**, *24*, 2582–2585.

[24] M. A. Fox, J. E. Harris, S. Heider, V. Pérez-Gregorio, M. E. Zakrzewska, J. D. Farmer, D. S. Yufit, J. A. K. Howard, P. J. Low, *J. Organomet. Chem.* **2009**, *694*, 2350–2358.

[25] L. J. Farrugia, *J. Appl. Crystallogr.* **2012**, *45*, 849–854.

[26] N. Arulsamy, D. S. Bohle, J. A. Imonigie, E. S. Sagan, *Inorg. Chem.* **1999**, *38*, 2716–2725.

[27] F. Neese, *Wiley Interdiscip. Rev.: Comput. Mol. Sci.* **2012**, *2*, 73–78.

[28] H. Walba, R. W. Isensee, *J. Org. Chem.* **1961**, *26*, 2789–2791.

[29] A.-R. Allouche, *J. Comput. Chem.* **2011**, *32*, 174–182.

[30] T. C. Berto, N. Xu, S. R. Lee, A. J. McNeil, E. E. Alp, J. Zhao, G. B. Richter-Addo, N. Lehnert, *Inorg. Chem.* **2014**, *53*, 6398–6414.

[31] C. G. Pierpont, R. Eisenberg, *Inorg. Chem.* **1973**, *12*, 199–205.

[32] G. Bombieri, E. Forsellini, R. Graziani, G. Zotti, *Transition Met. Chem.* **1977**, *2*, 264–267.

[33] C. Fellay, G. Laurenczy, S. M. Bischof, R. A. Periana, *Inorganic Syntheses, Vol. 35*, John Wiley & Sons, Inc., Hoboken, New Jersey, **2010**, pp. 152–155.

[34] G. Brauer, *Handbuch der Präparativen Anorganischen Chemie, Vol. 1*, Ferdinand Enke Verlag, Stuttgart, **1960**, pp. 481.

[35] G. M. Sheldrick, *Acta Crystallogr. Sect. A* **2015**, *71*, 3–8.

[36] G. M. Sheldrick, *Acta Crystallogr. Sect. C* **2015**, *71*, 3–8.

[37] W. Beck, H. Engelmann, H. S. Smedal, *Z. Anorg. Allg. Chem.* **1968**, *357*, 134–138.

[38] T. Mayer, W. Beck, H.-C. Böttcher, *Z. Anorg. Allg. Chem.* **2011**, *637*, 345–347.